Journal of The Electrochemical Society, 2022 **169** 044525

Finite Element Model Based Determination of Local Membrane Conductivity of Polymer Electrolyte Fuel Cells

A. Schuller,[1] T. J. Schmidt,[1,2,*] and J. Eller[1,,z]**

[1]*Electrochemistry Laboratory, Paul Scherrer Institut, Villigen PSI, 5232, Switzerland*
[2]*Laboratory of Physical Chemistry, ETH Zürich, 8093 Zürich, Switzerland*

A new non-invasive method to determine PEFC in-plane membrane conductivity distribution is proposed. It is based on electrical impedance tomography that relies on surface current injection and voltage measurement at the outer cell surface. The working principle is detailed and a numerical feasibility study shows the potential of the technique. Different conductivity profiles could be reconstructed based on synthetic boundary voltage data with a high accuracy. A sensitivity analysis was performed to understand the influence of different types of noise and error sources. This new method has the potential to become a relevant tool for fuel cell diagnostic if the required accuracy can be reached in terms of electrode positioning, cell characterization and measurement system.
 [DOI: 10.1149/1945-7111/ac6390]

Manuscript submitted November 18, 2021; revised manuscript received March 8, 2022. Published April 25, 2022.

Polymer Electrolyte Fuel Cells (PEFCs) are an essential technology for future, clean, fast-filling and long-range mobility. In large technical cells of a few hundred square-centimeter such as the ones used in automotive applications, water management is still an important challenge.[1] Indeed, due to the combination of the humidity in the inlet gases, and the water electrochemically produced, there tends to be an accumulation of water towards the outlet of the cell. This humidity gradient in the membrane may lead to detrimental consequences such as flooding or localized dry-outs. Additionally, the conductivity distribution gives important information regarding the state of health[2] of each individual cell as it also reflects the current density.[3] Hence, it is of great importance to have diagnostic tools able to provide information on the conductivity distribution in the membrane[4] to understand the influence of different operating parameters on the humidity distribution or to analyze the state of health of a stack after a long operating time for example.

There exist different techniques to retrieve information about the conductivity of the membrane being assembled in the cell.[5,6] Methods such as electrochemical impedance spectroscopy (EIS)[7] or high frequency resistance (HFR) measurement provide valuable information on the average resistance of the membrane. They can be used for a wide range of applications, from membrane electrode assembly (MEA) structure optimization to the study of the impact of different sorts of contamination.[8] EIS especially has proved to be an essential tool in PEFC research. However, this method only provides information on the average resistance of the membrane. Alternatively, methods such as segmented flow fields[9–12] or current shunt boards[13] can be used to provide information on the current distribution or the local impedance of the membrane. However, these methods are invasive, as they need an additional plate to be inserted within the fuel cell stack or modified flow field plates.

In this context, Electrical Impedance Tomography (EIT)[14] is proposed as an alternative technique to measure membrane conductivity distribution. This method is based on AC current injection and voltage measurement at the accessible outer surface area of the flow field plates. It is non-invasive and quickly adaptable to different stack designs, as it only needs surface attached electrodes. EIT has been used extensively in different fields. In medicine,[15,16] it has been successfully used to measure pulmonary functions in critical care units where non-invasive methods are the only possible options. Other applications also include geology and more generally industry where it is of interest to measure conductivity distribution in a non-invasive way.[17–19] For fuel cells, as an online diagnostic tool, EIT could be used to detect local flooding, localize dry-outs and more generally, follow the state of health of a fuel cell stack.

This manuscript describes the working principle of electrical impedance tomography and discusses how it can be applied to fuel cells. In order to demonstrate the capabilities of the approach, different possible conductivity distribution scenarios are reconstructed in a numerical feasibility study. Multiple conductivity scenarios, both 1D and 2D, are tested and different realistic humidity distributions corresponding to inlet-outlet gradients are reconstructed. Additionally, the limitations and some critical parameters of the technique for a future experimental application are discussed: the precision requirements on the a-priori knowledge of conductivity of the non-membrane cell components, the accuracy needed for electrode positioning, the acceptable level of signal noise and the influence of the flow field material.

Methodology

In the first subsection, the general working principle of EIT is detailed. It represents the ultimate goal of the application of EIT to fuel cells. In the second subsection, the numerical feasibility is introduced. It is meant as a first step in the application of EIT to fuel cells and aims at understanding the conditions in which EIT could be helpful for PEFCs diagnostic.

EIT working principle.—Electrical impedance tomography is based on the relationship that exists between one object's conductivity distribution and the surface potential that one can measure when an alternating current is applied to an object (see Fig. 1). This alternating current, in the range of a few mA and frequencies of up to 50 kHz, is injected between a pair of electrodes attached to the surface of the object. The resulting surface potential response is measured with an additional pair of electrodes. The repetition with many different pairs of injecting and measuring electrodes will produce a measurement dataset that allows to determine the actual conductivity distribution in the object. As shown on an example in Fig. 1a), current may be injected between electrodes 2 and 3 and the induced voltage is measured between all the other pairs of electrodes. Then the current is injected between electrodes 3 and 4 and the induced voltage is measured between all the other pairs of electrodes. This is repeated by injecting between electrodes 3 and 4, 4 and 5 and so on, all around the object. This so called adjacent stimulation pattern is the most commonly used one but any combination of electrodes may be used. As an alternative, the current may also be injected between electrodes 1 and 9 and the voltage measured between electrodes 7 and 8 as shown in Fig. 1b), called opposite stimulation pattern.

Equation 1, where σ is the conductivity and Φ the scalar potential, represents the continuum Kirchhoff's law. It is combined

*Electrochemical Society Fellow.
**Electrochemical Society Member.
[z]E-mail: jens.eller@psi.ch

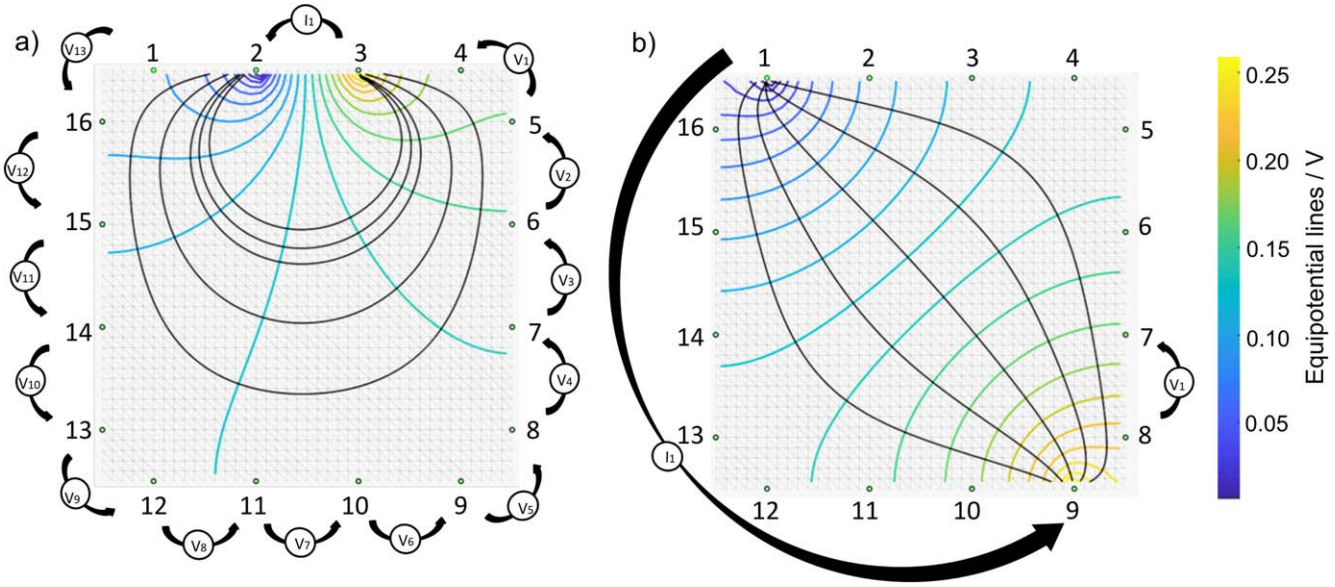

Figure 1. EIT working principle. The black lines correspond to the current streamline. The color bar shows the equipotential lines. The electrodes are numbered from 1 to 16. (a) adjacent stimulation pattern, (b) opposite stimulation pattern.

with a set of boundary conditions (Eqs. 2–4) that characterize the so-called Complete Electrode Model (CEM), which is the most complete form of the model to calculate the so-called EIT forward problem.[20] In this context, forward problem means calculating the boundary voltages with known current supply scheme and conductivity distribution in contrast to the inverse problem that aims at finding the conductivity distribution when the boundary voltages and the current supply scheme are known. Equations 2 and 3 correspond to the boundary conditions required at the electrodes where V_l is the voltage on the lth electrode E_l, z_l is the contact impedance of E_l, I_l is the current of the injecting electrodes and n is the outward unit normal to $\partial\Omega$, the boundary of the domain of interest Ω. Additionally, Eq. 4 requires that there is no current flow across the boundary of the system, where Γ is the boundary of the domain Ω besides all electrodes, $\Gamma = \partial\Omega - \sum E_l$. The equations are discretized and computed on a mesh of finite elements.

$$\nabla\cdot\sigma\nabla\Phi = 0 \qquad [1]$$

Boundary conditions:

$$\Phi + z_l\sigma\frac{\partial\Phi}{\partial n} = V_l \qquad [2]$$

$$\int_{E_l}\sigma\frac{\partial\Phi}{\partial n} = I_l \qquad [3]$$

$$\frac{\partial\Phi}{\partial n} = 0 \; on \; \Gamma \qquad [4]$$

Solving Eq. 1 and the associated boundary conditions (Eqs. 2–4) with a given conductivity profile and stimulation pattern leads to the solution of the forward problem, including the boundary voltage at the electrodes corresponding to each stimulation. However, it is the inverse problem of the problem of interest. Indeed, the goal of EIT is to physically apply the stimulation patterns on the device under test, to collect the boundary voltages, and to calculate back the conductivity distribution in the reconstruction step. In other fields where EIT is used, such as medicine, the preferred method for conductivity reconstruction is mostly solving the inverse problem numerically.[20] However, the inverse problem is usually mathematically ill-posed;[21] there may not be a unique conductivity distribution for a given set of surface voltage measurements and for large finite element problems this solution approach becomes numerically very challenging.

For PEFC application we take advantage of the fact of prior knowledge about the conductivity of fuel cell components with known conductivity. Indeed, the dominating change in conductivity while operating the cell is expected to take place in the ionomer: the conductivity of the other layers of the fuel cell can, therefore, be set in advance and the only unknown is the membrane conductivity. Additionally, to further simplify the problem, the through-plane conductivity is assumed to be locally homogeneous such that the conductivity profile in the membrane is approximated as a 1D or 2D interpolation between a few interpolation points in the in-plane direction to limit the number of degrees of freedom.

The reconstruction is based on an optimization formulation that aims to minimize the deviation between the surface potentials predicted by the finite element model and the measured surface potentials for the different stimulation patterns.[22,23] In a first step, an initial conductivity profile is assumed to be a constant value. The corresponding surface potentials φ_{calc} are then calculated with the model and compared to the experimentally determined voltages φ_{meas}. An optimizer, based on a covariance matrix adaptation evolutionary strategy,[24] is used to minimize the difference between the experimental and calculated voltages by varying the conductivity distribution and recalculating the boundary voltages until a certain threshold error has been met (see Eq. 5). The final conductivity profile that is obtained after convergence of the optimizer is therefore the one corresponding to the one in the actual fuel cell.

$$\min\left(\varphi_{calc} - \varphi_{meas}{}^2\right) \leqslant threshold \qquad [5]$$

Numerical feasibility study.—In order to assess if EIT could be applied to fuel cells, a numerical feasibility study has been performed for different conductivity distribution scenarios. Instead of using real measured surface potentials φ_{meas}, the finite element model is used to calculate synthetic measurement data φ'_{meas} for specific membrane conductivity distributions. A 3D mesh based representation of a simplified fuel cell geometry (see Fig. 2) is created and the respective conductivity is assigned to each finite element. The forward problem is solved for the whole PEFC model for each conductivity distribution described below. Each forward solution yields a synthetic measurement set which can be fed to the reconstruction algorithm, which uses trials to reconstruct the

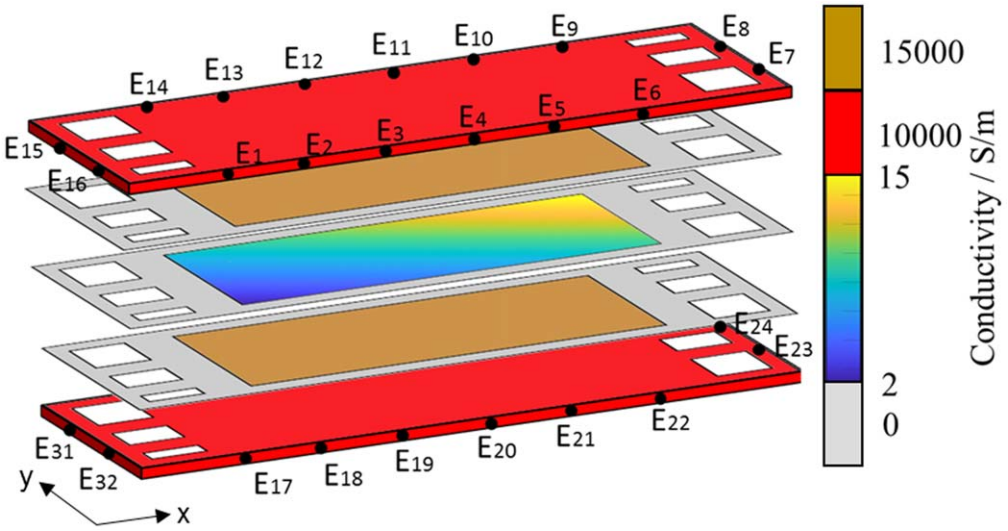

Figure 2. Simplified PEFC model with (from top to bottom) flow field plate, gas diffusion layer (GDL) and gasket, membrane and gasket, GDL and gasket, flow field plate and their corresponding conductivity in the color bar. Electrodes (E1 to E32) positions are marked in black dots.

conductivity distribution only by matching the surface potentials. The quality of the reconstruction is assessed by comparing the original conductivity distribution used to solve the forward problem with the reconstructed conductivity distribution. For this study, the MATLAB software package EIDORS[25] is used to solve the forward problem (Eqs. 1–4) with a finite element approach. EIDORS, which stands for electrical impedance tomography and diffuse optical tomography reconstruction software, is a free and open source software toolkit dedicated to EIT problems. It is able calculate the EIT forward problem for 2D and 3D geometries on a finite element mesh, a conductivity associated to each element, electrodes locations and stimulation patterns. Additionally, it is able to solve the inverse problem for simple 2D and 3D geometries, i.e. for biomedical applications. For postprocessing EIDORS offers visualization tools to analyze the conductivity distribution, the current distribution in the investigated object and the isopotential lines. Table I describes the different important parameters used in the calculations.

The different tested conductivity profiles displayed in Fig. 3 are listed below (x and y are the direction along and across the channel, respectively):

a) 1D linear: $\sigma(x) = (0.0442 \cdot x - 2.74)$ S/m
b) Cubic: $\sigma(x) = (8.0272\text{e-}10 \cdot x3 - 5.3308\text{e-}07 \cdot x2 + 7.7453\text{e-}05 \cdot x + 0.0066)$ S/m
c) RH profile based on experimental measurement of the humidity in an operating counter-flow cell[26] and the link between specific conductivity and Nafion water uptake.[27]

Table I. Description of the parameters for the numerical feasibility study.

Parameters	Value
Current	20 mA
Number of electrodes	32 (16 per flow field)
Stimulation pattern	adjacent
Flow field thickness	2.2 mm
Flow field conductivity	10 S mm^{-1}
Active area	200 cm2
GDL thickness	150 um
GDL conductivity	15 S mm^{-1}

d) 2D linear: $\sigma(x) = (1.766\text{e-}05 \cdot x + 3.637\text{e-}05 \cdot y)$ S/m

Inlet to outlet 1D conductivity gradients are typical for fuel cell operation with parallel flow field as water tends to accumulate at the cathode outlet. Moreover, 2D gradients such as the one shown in Fig. 3d) are typical for serpentine flow fields.

Additionally, different kinds of noise and error sources are implemented in order to understand their impact on the quality of the reconstructed conductivity distribution. First, the level of precision needed in the *a priori* knowledge of the cell conductivity is tested by adding an error of 0.1 to 1 percent in flow field conductivity in the reconstruction. Second, the influence of misplaced electrodes is

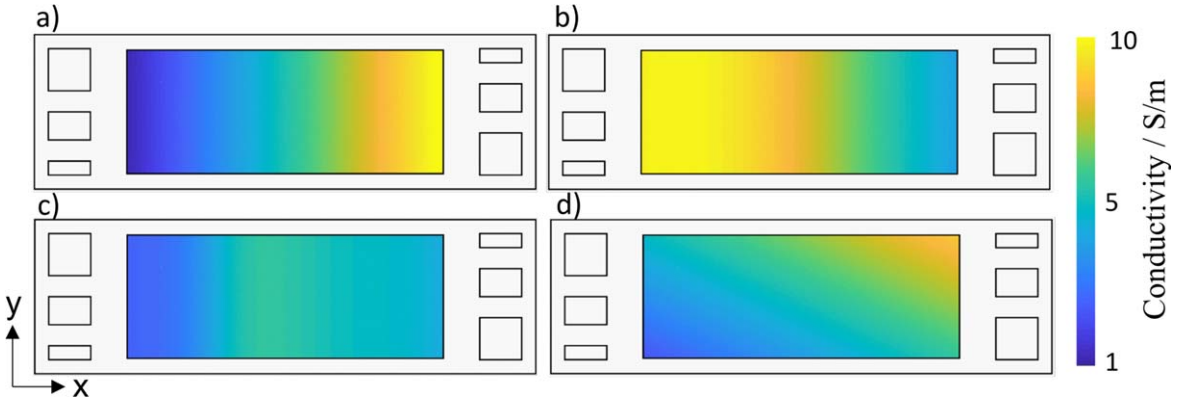

Figure 3. Conductivity profiles used as test scenarios in the numerical feasibility study: (a) 1D linear, (b) 1D cubic, (c) 1D real RH profile, (d) 2D linear

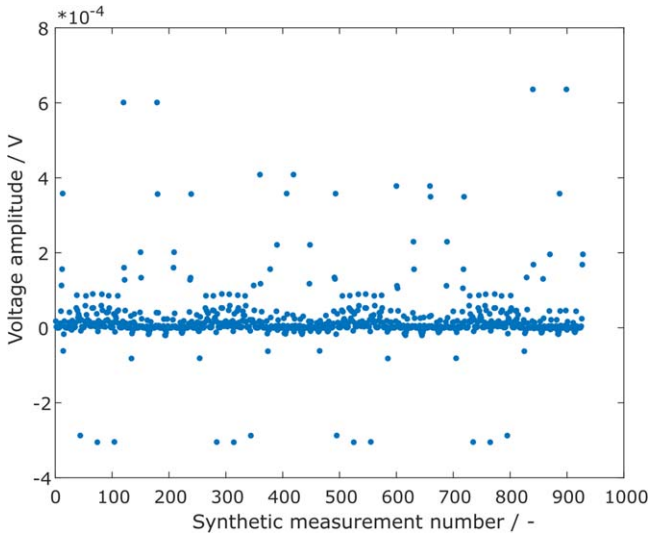

Figure 4. Voltage measurements data for an adjacent stimulation pattern; each synthetic measurement represents a specific combination of injection and measurement electrodes.

investigated by running the reconstruction process on a model with randomly shifted electrodes by 0.5 to 5 mm along the width or length of the flow field. Third, different levels of Gaussian noise are incorporated in the synthetic measurement data before the reconstruction.

An analysis of the current path through the membrane is provided to discuss the difference between different flow field materials for EIT applications. The flow fields of PEFCs are usually made of either graphite or stainless steel. Indeed, for stationary applications where the stack volume is less important, graphite can be used. However, for automotive applications where weight and volume are crucial parameters, stainless steel is preferred as it enables a higher volumetric power density. These materials differ greatly in conductivity which also lead to stainless steel flow fields being thinner. As for EIT application, the electrodes directly contact the surface of the flow fields, their materials have an important impact because the supplied current would follow different paths depending on the conductivity and thickness of the flow field. For this reason, two different flow field materials are investigated in terms of current pathways. The first one is graphite with a conductivity of 10 S mm^{-1} and the second is stainless steel with a conductivity of 1000 S mm^{-1}. The values chosen here are not meant to correspond precisely to a specific value of the conductivity of a product or material from a specific manufacturer but rather represent the order of magnitude of

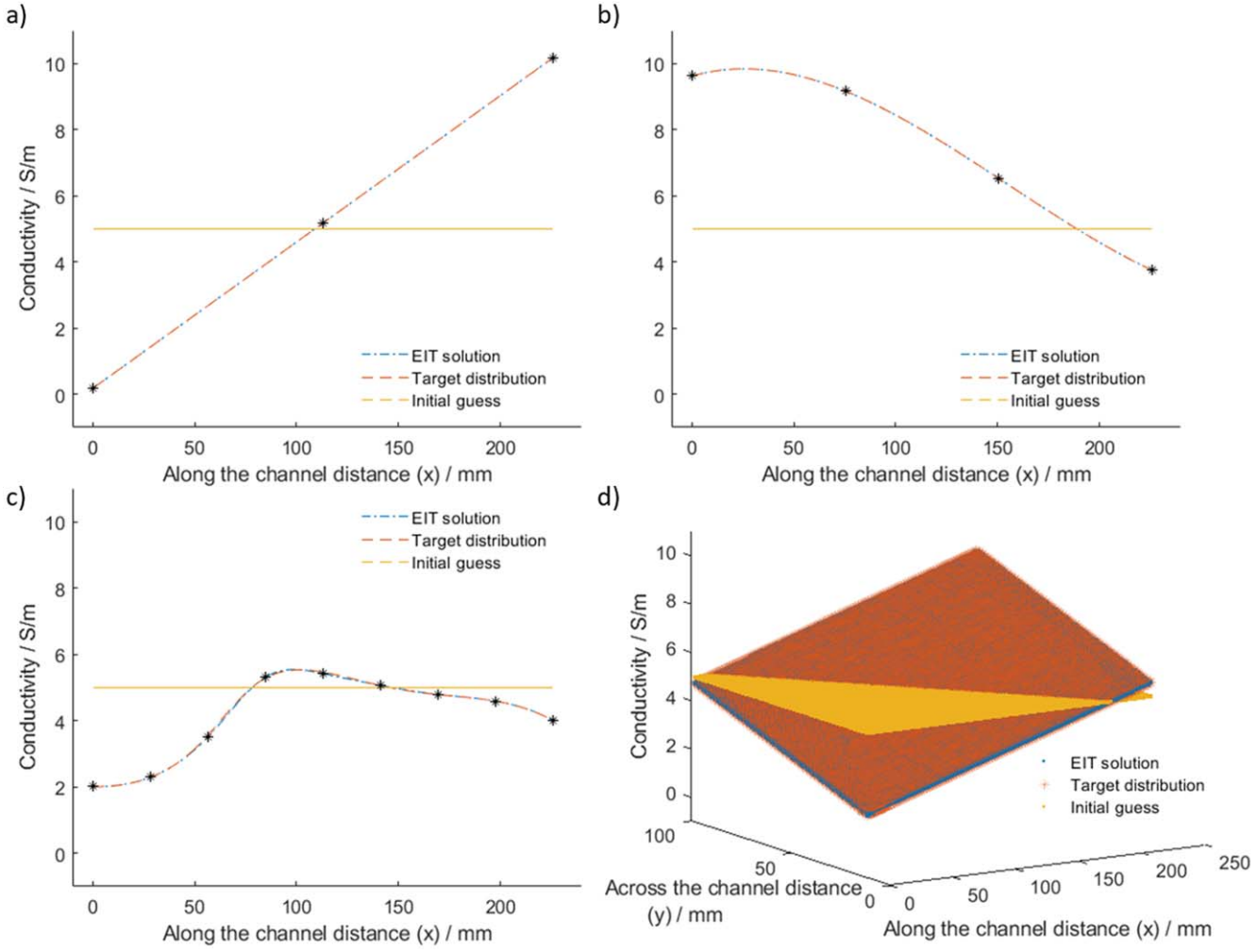

Figure 5. Reconstructions of different conductivity distributions scenarios. (a) 1D linear, (b) 1D cubic, (c) 1D real RH profile and (d) 2D linear; the yellow horizontal line represents the initial conductivity guess (the starting point of the minimization process), the red dashed line is the conductivity profile of the different scenarios, the blue dashed line is the result of the minimization process and the stars correspond to the location and value of the interpolation points.

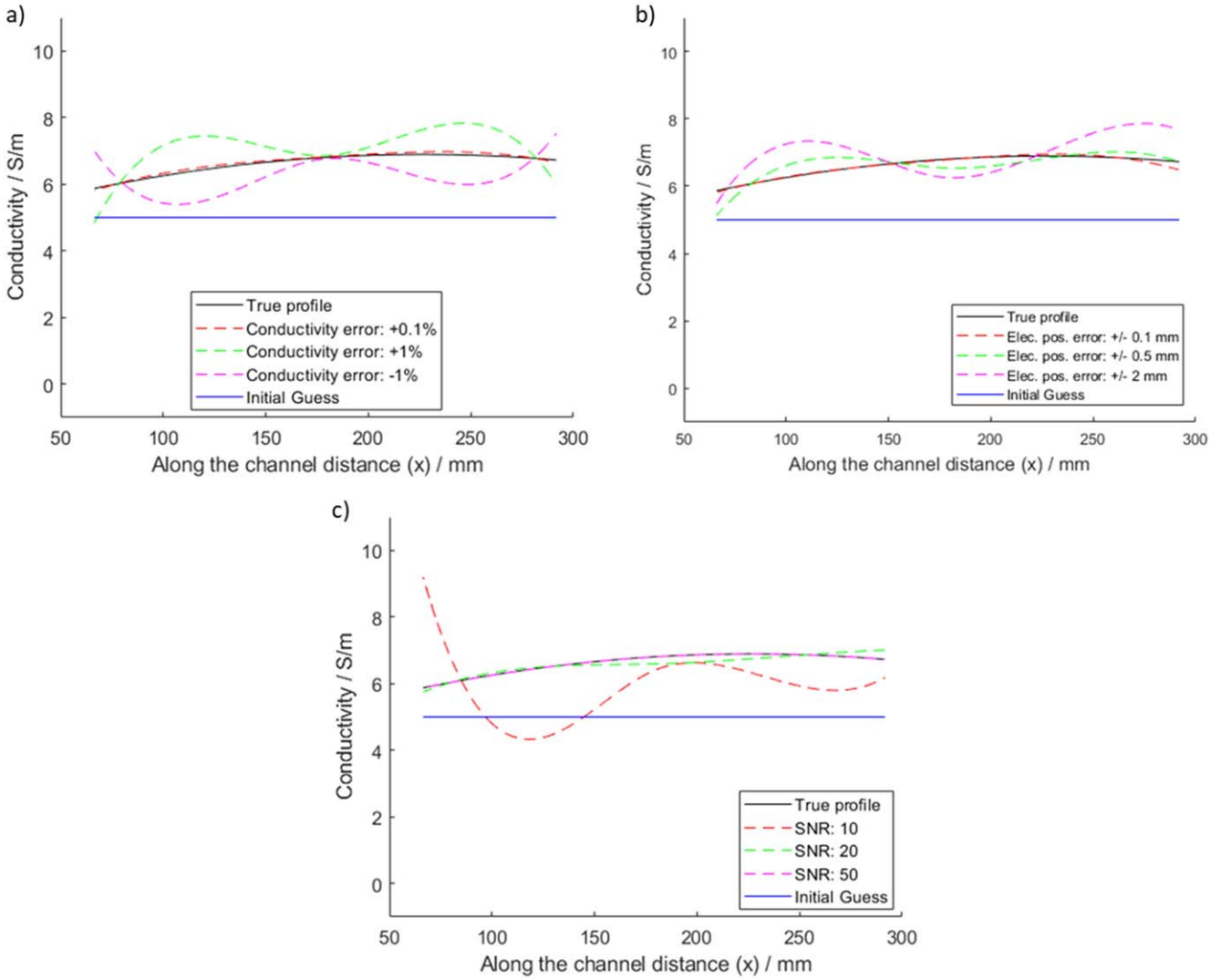

Figure 6. Impact of several kinds of error sources and noises on the reconstruction quality. (a) the assumed conductivity of the flow field in the model is assumed wrong by +/− 1% and + 0.1% (b) the electrodes positions are shifted by 0.1, 2 and 5 mm (c) the signal to noise ratio is set to 10, 20 and 50 dB.

the relative ratio between the two materials in terms of conductivity and thickness difference.

Results and Discussion

The synthetic voltage data corresponding to an adjacent stimulation pattern of the conductivity test scenario a) is shown exemplarily in Fig. 4. The simulated voltage amplitudes that can be expected in real measurements are in the range of a few microvolts to some hundred microvolts. These values are in a much lower range than what is usually observed for EIT[14] and handled with EIDORS, as the conductivities are much higher than the ones found in biological applications for example. The distribution with high values followed by low values is typical for the adjacent stimulation pattern. Indeed, when current is supplied between two neighboring electrodes, the induced voltage tends to be higher in the nearby region and fade away rapidly. This explains why there are voltage peaks and why most of the values are very low. Additionally, some voltage values are positive and some are negative. This depends on the relative position of the positive and negative voltage measurement electrodes to the positive and negative current injecting electrodes.

The reconstruction of the membrane conductivity profiles for the different test scenarios is shown in Fig. 5. For all of the cases the match is excellent, even though the surface voltages are quite small. For case a), three interpolation points are enough to fit the simple linear case. The cubic case b) requires four points to reach a good match. The match is also excellent when the number of interpolation points and therefore the resolution is high, such as for the counter flow RH distribution shown in Fig. 5c) which requires nine interpolation points. Finally, case d) requires two interpolation points in each direction to reach a good match. EIT seems therefore to be a promising tool for PEFC diagnostic.

However, the very nature of such a numerical feasibility study comprises several assumptions and a number of parameters, which may differ from reality or may not be so precise under control in reality. Potential deviation from reality therefore have to be taken into account in the feasibility study to guide future experimental work. Three different kind of error sources and their influence on the accuracy of the reconstructed conductivity profile are discussed here: an error in the assumed conductivity of one of the parts of the cell, a mismatch between the electrode position in the model and in the experiment and finally random noise coming from the instrumentation (see Fig. 6). First, if the actual conductivity differs from the one assumed in the model, the path the current will follow might not be the same for certain stimulation patterns. This will lead to a different induced voltage, which eventually translates into a possible error in the reconstructed conductivity distribution. As only the membrane conductivity distribution is reconstructed, the result will be

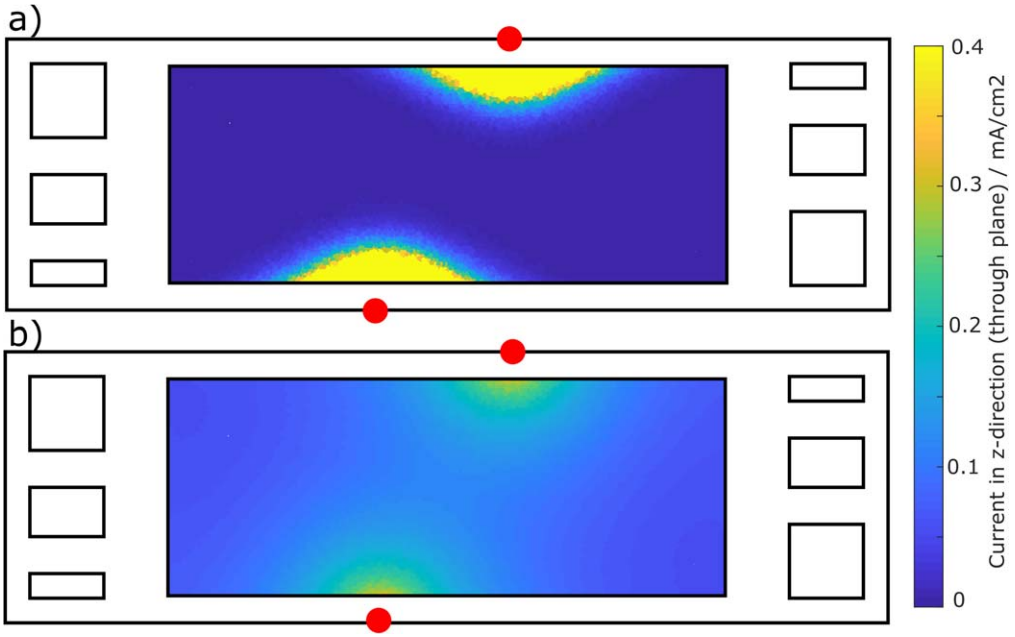

Figure 7. Cross section of a simplified fuel cell geometry showing where the current crosses the membrane for graphite (top) and stainless steel (bottom). The red dots represent the locations of the electrodes where the current is injected and sinked.

compensated for any discrepancy between the model conductivities and the experimental ones. This simulated error takes only into account a homogeneous misrepresentation of the conductivity which would not necessarily be the case in a real scenario. The impact of such an error is displayed in Fig. 6a). An error of 1% already induces an error of around 1 S m^{-1} and significantly changes the shape of the conductivity distribution curve. Additionally, the reconstructed profile is affected differently if the conductivity is overestimated or underestimated. On the other hand, an error of 0.1% is sufficient for a correct reconstruction.

A mismatch between model and experiment regarding the position of the electrodes would also influence the path of the current and eventually lead to different measured boundary voltages and therefore a different reconstructed conductivity distribution. The impact of such an error is displayed in Fig. 6b). Its impact is critical: a difference of a few millimeters in electrodes positions leads to an error above 1 S m^{-1}. A positioning error of 0.5 mm would lead to errors still up to 0.5 S m^{-1} while keeping a correct trend. A low error of 0.1 mm would lead to an average error below 0.1 S m^{-1} and a very good fit. For a real electrodes positioning system, an error around 0.1 mm would be preferable.

Finally, as shown in Fig. 4, the voltage readings are quite low. It is important to note that the average difference between those four cases is in the order of a few microvolts (for 20 mA current stimulation). The accuracy of the data acquisition system characterized by its signal to noise ratio (SNR) is therefore very important. Figure 6c) shows the impact of different SNRs on the reconstruction quality. A SNR of 20 dB means that the value of the signal is higher than the noise by a factor of 100 ($10^{\frac{20dB}{10}}$). A SNR of 10 dB is not enough, inducing errors of up to 3 S m^{-1} while a SNR of 20 dB is already sufficient: a SNR of 50 dB does not improve the reconstruction much further. Here it is also important to note that with a data acquisition system measuring a voltage sine, the accuracy for the single measured voltage points does not need to have a SNR of 20 dB: as multiple current sines would be supplied, a voltage sine would be fitted and averaged, which would increase the accuracy.

Additional mismatches to the error sources listed above should also be considered. The contact resistance between the different layers of the cell (and depending on cell compression and materials), which may not be homogeneous, would need to be incorporated in the model to accurately represent reality. The geometry and its mesh used in the finite element model also have to be precisely designed. The model assumes isotropy of the materials properties which would also need to be taken into account. Overall, it is clear from these figures that a quite precise match is needed between the experimental and modeled conditions and parameters to use this technique as an experimental diagnostic tool for PEFCs.

Another challenge of the technique regards its sensitivity in spatial resolution towards the center of the cell. Figure 7 shows the cross section of a simplified fuel cell geometry with a color map of where and how much current crosses the membrane for different cases: a) the flow fields have a conductivity corresponding to graphite and b) the flow fields have a conductivity corresponding to stainless steel. In case of the graphite flow field, most of the injected current crosses the membrane very locally close to the injecting electrodes (see Fig. 7a). It corresponds to roughly 50% of the current crossing in 5% of the surface area and 90% of the current crossing in 20% of the surface area. This makes the current probe the membrane very locally and only near the flow field walls. However, in case of the stainless steel flow field plates with increased in-plane conductivity, the current tends to spread over the flow field plate and the through plane currents distribute more evenly on the membrane surface (see Fig. 7b). It corresponds to 50% of the current cross in 40% of the surface area and 90% of the current crossing in 85% of the surface area. On the one hand, graphite seems appropriate to yield strong signal with very local information as the current does not spread in the flow field plane. However, it means that the membrane conductivity is mainly probed in the area close to the injecting electrode and that the determination of the membrane conductivity in the center of the cell by EIT will be challenging. On the other hand, stainless steel, which is the main flow field material in the automotive applications, allows the current to spread all across the membrane. Each stimulation pattern would therefore hold less strong local information but with measurements all around the membrane, the inner part of the membrane would be more accessible.

Conclusions

Electrical impedance tomography is proposed as a non-invasive tool for the determination of the in-plane membrane conductivity in polymer electrolyte fuel cells. In this numerical feasibility study it could be shown that EIT is applicable to fuel cell dimensions and

material conductivities and that the incorporation of a-priori knowledge of non-ionic conducting cell components into the solution process is possible. In order to reduce the degrees of freedom the membrane conductivity is assumed to be constant over the membrane thickness and described by 1D or 2D parameterizations.

The reconstructed conductivity profiles showed a very good match to the assumed test scenario conductivity distributions and the method could resolve a complex 1D inlet to outlet gradient with a resolution below 3 cm. However, an analysis of the possible differences between experiments and model results showed that the model needs to be very accurate in order for the method to be precise enough. The conductivity of each component of the fuel cell needs to be precisely characterized and that information has to be fed into the model. An error well below 1% in assumed conductivity seems to be required to have a correct reconstruction. The electrodes also need to be positioned with an error of around 0.1 mm which can be achieved by a clever engineering solution. Finally, a data acquisition system has to be designed and has to meet the following basic requirements: it has to have multiple channels in order to be able to measure all around the cell at the same time and it requires a voltage fitting accuracy of about 20 dB for absolute voltage values of around 100 μV. The analysis of the current path through the membrane offered insights into challenges and opportunities of the two main flow field materials. Graphite can help EIT to provide strong local information at the expense of 2D resolution while stainless steel would help EIT to provide better 2D resolution at the expense of more smeared out weaker local information.

Since it seems possible to meet the requirements with available instrumentation, EIT would be an ideal tool for PEFC diagnostic as it would be able to provide local information on the membrane conductivity distribution in a non-invasive way and replace invasive shunt resistor based stack inserts. EIT can address various topics like optimization of the inlet RH conditions, local cell defects and degradation, optimization of flow field geometries to achieve a homogeneous conductivity distribution, higher efficiency and increased life time. Due to the instrumentation requirements, EIT will be most likely applied in research and development environments, but also automotive service applications or even onboard implementations might be possible. Proof of concept experiments are currently being performed to establish EIT as a noninvasive locally resolved diagnostic tool for PEFCs.

Acknowledgments

The authors would like to acknowledge the Swiss Federal Office of Energy (SFOE) for financial support under grant no. 501860-01 and Valentina Stampi-Bombelli for EIDORS model development and testing.

ORCID

A. Schuller https://orcid.org/0000-0001-5516-6743
T. J. Schmidt https://orcid.org/0000-0002-1636-367X
J. Eller https://orcid.org/0000-0002-9348-984X

References

1. Y. Wang, K. S. Chen, J. Mishler, S. C. Cho, and X. C. Adroher, *Appl. Energy*, **88**, 981 (2011).
2. N. Fouquet, C. Doulet, C. Nouillant, G. Dauphin-Tanguy, and B. Ould-Bouamama, *J. Power Sources*, **159**, 905 (2006).
3. J. Stumper, S. A. Campbell, D. P. Wilkinson, M. C. Johnson, and M. Davis, *Electrochim. Acta*, **43**, 3773 (1998).
4. M. M. Mench (ed.), *in Fuel Cell Engines* (Wiley, Hoboken, NJ) p. 453 (2008).
5. X. Yuan, H. Wang, J. Colin Sun, and J. Zhang, *Int. J. Hydrogen Energy*, **32**, 4365 (2007).
6. K. R. Cooper and M. Smith, *J. Power Sources*, **160**, 1088 (2006).
7. T. E. Springer, T. A. Zawodzinski, M. S. Wilson, and S. Gottesfeld, *J. Electrochem. Soc.*, **143**, 587 (1996).
8. X.-Z. Yuan, C. Song, H. Wang, and J. Zhang, *Electrochemical Impedance Spectroscopy in PEM Fuel Cells* (Springer, London) (2010).
9. N. Rajalakshmi, *J. Power Sources*, **112**, 331 (2002).
10. S. J. C. Cleghorn, C. R. Derouin, M. S. Wilson, and S. Gottesfeld, *J. Appl. Electrochem.*, **28**, 663 (1998).
11. S. A. Freunberger, I. A. Schneider, P.-C. Sui, A. Wokaun, N. Djilali, and F. N. Büchi, *J. Electrochem. Soc.*, **155**, B704 (2008).
12. I. A. Schneider, H. Kuhn, A. Wokaun, and G. G. Scherer, *J. Electrochem. Soc.*, **152**, A2383 (2005).
13. SPLUS, (accessed February 18, 2019), http://splusplus.com/measurement/en/cslin.html.
14. L. R. Price, *IEEE Trans. Nucl. Sci.*, **26**, 2736 (1979).
15. I. Frerichs, *Physiol. Meas.*, **21**, R1 (2000).
16. B. H. Brown, D. C. Barber, and A. D. Seagar, *Clin. Phys. Physiol. Meas.*, **6**, 109 (1985).
17. T. York, *J. Electron. Imaging*, **10**, 608 (2001).
18. P. G. Kaup and F. Santosa, *J Nondestruct Eval*, **14**, 127 (1995).
19. F. J. Dickin, R. A. Williams, and M. S. Beck, *Chem. Eng. Sci.*, **48**, 1883 (1993).
20. W. Lionheart and A. Adler, *Electrical Impedance Tomography Methods, History and Applications* (CRC Press, Boca Raton, FL)p. 5 (2021).
21. T. Murai and Y. Kagawa, *IEEE Trans. Biomed. Eng.*, **BME-32**, 177 (1985).
22. S. Martin and C. T. M. Choi, *IEEE Trans. Magn.*, **52**, 1 (2016).
23. S. Pravin Kumar, N. Sriraam, P. G. Benakop, and B. C. Jinaga, *2010 5th International Conference on Industrial and Information Systems* (IEEE, Piscataway, NJ) p. 339 (2010).
24. N. Hansen and S. Kern, *Parallel Problem Solving from Nature - PPSN VIII*, ed. X. Yao et al. (Springer, Berlin) 3242, p. 282 (2004).
25. N. Polydorides and W. R. B. Lionheart, *Meas. Sci. Technol.*, **13**, 1871 (2002).
26. S. Kreitmeier, G. A. Schuler, A. Wokaun, and F. N. Büchi, *J. Power Sources*, **212**, 139 (2012).
27. T. A. Zawodzinski, T. E. Springer, J. Davey, R. Jestel, C. Lopez, J. Valerio, and S. Gottesfeld, *J. Electrochem. Soc.*, **140**, 7 (1993).